RESEARCH ON EXTERNAL AERODYNAMICS OF THE HIGH-SPEED POWERED EXPERIMENTAL FLIGHT TEST VEHICLE WITHIN THE HEXAFLY-INT PROJECT

A.A. Gubanov, N.V. Voevodenko, V.A. Talyzin, D.S. Ivanyushkin, A.O. Podosinnikov and V.A. Yakovleva *
* Central Aerohydrodynamic Institute named after Professor N.E. Zhukovsky (TsAGI), Russian Federation

Keywords: *high-speed aerodynamics, CFD, EFD, test vehicle*

Abstract

CFD and EFD studies of the aerodynamics of the high-speed civil aircraft model HEXAFLY-INT have been performed in wide range of Mach numbers, angles of attack and slip angles. It was shown that the characteristic feature of this intake is the occurrence of subsonic separation zone in the central part of the flow. The obtained results made it possible to create the aerodynamic database of the HEXAFLY-INT EFTV model in a wide range of parameters.

1 Introduction

The European Community (EC) co-funded international project HEXAFLY-INT is aimed at the development of technologies for creation of the high-speed passenger vehicle able to make an antipodal flight within 3 hours. The basic vehicle concept under study is the LAPCAT MR-2 vehicle shown on Fig. 1 which had been developed in previous EC co-funded projects ATLLAS I & II, LAPCAT I & II [1] [2]. It is a high-speed passenger aircraft to cruise at Mach 8. The currently on-going project HEXAFLY-INT includes study of the two concepts of the experimental flight test vehicle (EFTV) based on the LAPCAT MR-2 vehicle concept: the powered one developed within the preceding project HEXAFLY [3], and the glider. The EFTV powered concept is under study within the HEXAFLY-INT project just by Russian partners and includes CFD research and wind-tunnel tests. Investigations on the EFTV glider concept are being provided by all the partners of the HEXAFLY-INT project, i.e. European, Russian and Australian entities, and include CFD, wind-tunnel and flight tests. The current paper presents CFD and experimental research on aerodynamics of the EFTV powered concept provided by TsAGI.

Fig. 1. The basic configuration of the LAPCAT MR-2 passenger vehicle

The general view of the EFTV powered vehicle is shown in Fig. 2. The vehicle has a waverider bottom surface, two vertical fins and a dorsal mounted inward-turning air intake with elliptical cross section described in [4].

Computations were made with the aim to create an aerodynamic database (AEDB) for the vehicle, and the wind-tunnel tests were provided in order to verify the CFD aerodynamic data and to check whether the flow pattern predicted by CFD does really take place in the wind-tunnel test conditions.

Computations of the EFTV aerodynamics were carried out in two stages: at the first stage of numerical studies, calculations were performed using methods based on the solution of Euler's equations and simple engineering methods; in the second stage, CFD modeling

was performed by more complicated methods based on the solution of the averaged Navier – Stokes equations (RANS). The application of various methods for the external aerodynamics calculations allowed 1) increasing the reliability and validity of the results, 2) determining the applicability areas of the applied methods, and 3) optimizing the distribution of computing resources, using simple, fast and robust methods where possible.

2 Vehicle geometry

EFTV propelled model geometry shown in Fig. 2, is a version of the experimental vehicle developed under LAPCAT-MR2 program as a conceptual design of hypersonic passenger aircraft to cruise at Mach 8 with an overhead inverted air intake. The bottom surface of the vehicle has a form of waverider, designed for cruising Mach number = 7 ÷ 8.

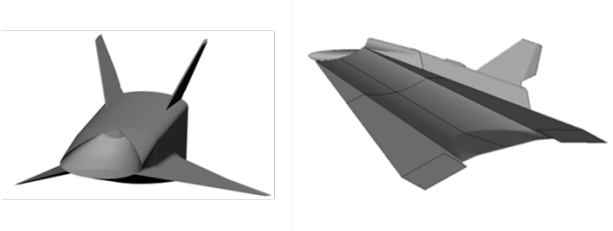

Fig. 2. General view of the EFTV powered concept

The EFTV air intake has a complex convergent geometry obtained as a result of modification of the surface known as the Busemann diffuser, the theoretical solution described in the book [5]. The shape of the deceleration surface extends along the flow lines of the conical flow and allows isentropic braking of the flow. The intake shape is described in more details in [7].

3 CFD studies

This section presents the results of numerical studies of flow and aerodynamic characteristics of the HEXAFLY-INT EFTV propelled model.

Computations of the EFTV aerodynamics were carried out in two stages: at the first stage of numerical studies, calculations were performed using methods based on the solution of Euler's equations and simple engineering methods; in the second stage, CFD modeling was performed by more complicated methods based on the solution of the averaged Navier – Stokes equations (RANS). The application of various methods for the external aerodynamics calculations allowed 1) increasing the reliability and validity of the results, 2) determining the applicability areas of the applied methods, and 3) optimizing the distribution of computing resources, using simple, fast and robust methods where possible.

Calculations of external aerodynamics at the first stage were performed, basically, for the wind tunnel T-116 conditions in the range of parameters: M_∞=2 ÷ 10 with the step 1, Re = 5.38 ÷ 7.66·10^6, AoA = -16° ÷ 16°, step 2°, AoS = 0 ° ÷ 4 °, step 2°, ailerons deflection angle δ = -16° ÷ 16°, step 4°, for the purpose to compare the results and validate the numerical methods. At the second stage, the regime conditions matrix was compiled corresponding to the flight conditions at an altitude of about 30 km: M∞ = 2 ÷ 7.5, Re = 3. ÷ 12·10^6 at α = -4° ÷ 12°, β = 0 ÷ 2°, δ = -5°, -10°.

RANS numerical simulation of the external flow and of the flow in the air intake area up to the engine duct entrance section was always performed by using the software package ANSYS FLUENT. Further, the flow inside the engine duct was simulated with the FLUENT package only for modes without fuel supply and combustion. To simulate the modes with fuel combustion inside the engine duct, we used own packages, developed in TsAGI and CIAM.

3.1 CFD tool

CFD simulation was performed using ANSYS FLUENT commercial package, which is designed to simulate complex flows over a wide range of velocities.

One of the most crucial and important stages in the simulation of high-speed gas dynamic problems is the construction of a computational grid, especially inside the shock layer. From its quality and structure often depends on the correctness and accuracy of the resulting solution.

The complexity of the aerodynamic configuration required the use of grids of large size. The computational grid was formed in three stages. At the first stage, a non-structured triangular grid was built on the surface of the model, and it was checked for errors and elements with poor quality. If necessary, adaptation of the surface grid for a more accurate description of the elements of the model was carried out. At the second stage, to compute the flow in the boundary layer on the surface grid, a layer of prismatic elements was built up (the height of the first layer of prisms corresponded to the value Y + = 1), after which the grid was re-aligned. At the final stage, the inner volume of the computational domain was filled with tetrahedral cells with a build-up coefficient of 1.2. The dimension of the computed grid was 40 000 00 cells. In calculations with a zero slip angle, the grid was constructed for the model half with the symmetry condition along the right boundary of the computational domain. The grid volume in this case was 20 000 000 cells. An example of a computational grid is shown in Fig. 3.

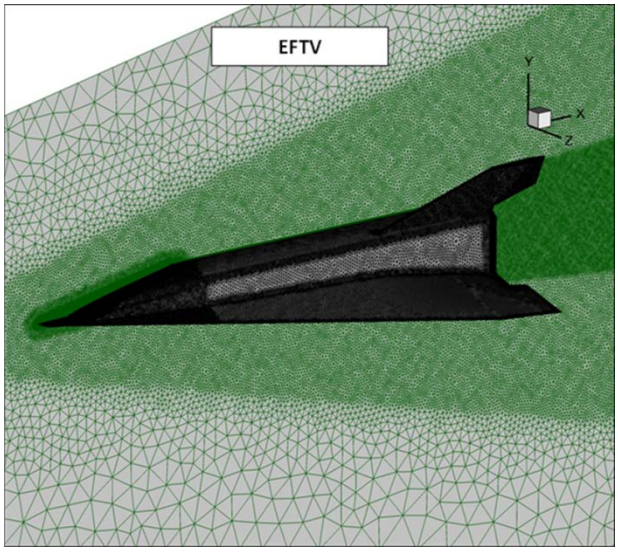

Fig. 3. Numerical grid

The computational studies of the EFTV HEXAFLY-INT aerodynamic characteristics are performed by the time-based relaxation method, within the framework of the Reynolds averaged Navier-Stokes equations closed by the Spalart-Allmaras (SA) turbulence model. SA turbulence model is low-Reynolds and is applied in the entire design area, including zones near solid walls, on which, as the boundary condition, $\nu_{œ} = 0$ is assumed. In this case, near the solid surfaces, it is required a numerical grid that provides a sufficiently large number of elements within the boundary layer and within a viscous sublayer. However, the FLUENT package provides the possibility to use the wall functions, if the grid resolution in the near-wall region is not large enough. SA model is efficient and accurate enough for the calculation of flows with not very large separation zones.

In the computations, the implicit method of solution was predominantly used with increasing Courant number during the course of the flow stabilization. The size of the computation domain was chosen from the condition that the external boundaries, on which the free-stream flow conditions were set, do not influence on the solution. On a solid surface, adhering conditions were fulfilled. Also on the body of the aircraft were set parameters of radiation from aerodynamic heating of the surface. On the surface of the elevons, the radiation coefficient corresponded to the value $\varepsilon = 0.8$, and on the rest of the body the value $\varepsilon = 0.4$. In average from 15,000 to 20,000 iterations were required to achieve the convergence and obtain a steady-state stationary solution.

3.2 CFD results

As a result of the studies, the total coefficients of aerodynamic forces - C_x, C_y, C_z, and of moments m_x, m_y, m_z acting on the aircraft, as well as the air flow rate f, are obtained. In calculating of aerodynamic coefficients C_x, C_y, C_z, the values of the aerodynamic forces X, Y, and Z are referred to the free-stream dynamic pressure and to the characteristic area $S_{ref} = 2.44$ m^2. In determining of the coefficients of rolling moment m_x, yaw moment m_y and pitch moment m_z, the magnitude of the aerodynamic moments Mx, My, Mz are referred to the free-stream dynamic pressure, to the characteristic area $S_{ref} = 2.44$ m^2 and the span of the wing b = 1.24 m for the moments of roll and yaw and to the characteristic length $L_{ref} = 2.876$ m for the

moment of pitch. The moments were calculated relative to the conditional center of mass located at a distance of 0.57 L_{ref} from the leading edge of the model. The flow rate coefficient f was calculated for the characteristic intake area S_{int} = 0.042 m^2. The conditional section of the intake entrance was located at a distance of 0.301 L_{ref} from the leading edge.

Numerical simulation was carried out in the range of Mach numbers M = 2 ÷ 7.5 and angles of attack α = -4 ° ÷ 12 ° at slip angles β = 0 and 2 °. The Reynolds number was calculated on the model body and corresponded to the values:

- $Re_L=9.97*10^6$ for M=2
- $Re_L=6.69*10^6$ for M=4
- $Re_L=9.38*10^6$ for M=6
- $Re_L=1.06*10^7$ for M=7
- $Re_L=3.17*10^6$ for M=7.5

Next, the results of numerical simulation of the flow of EFTV are considered. Dependences of the aerodynamic forces and moments coefficients of on the angle of attack α are shown for M = 7 in Fig. 4.

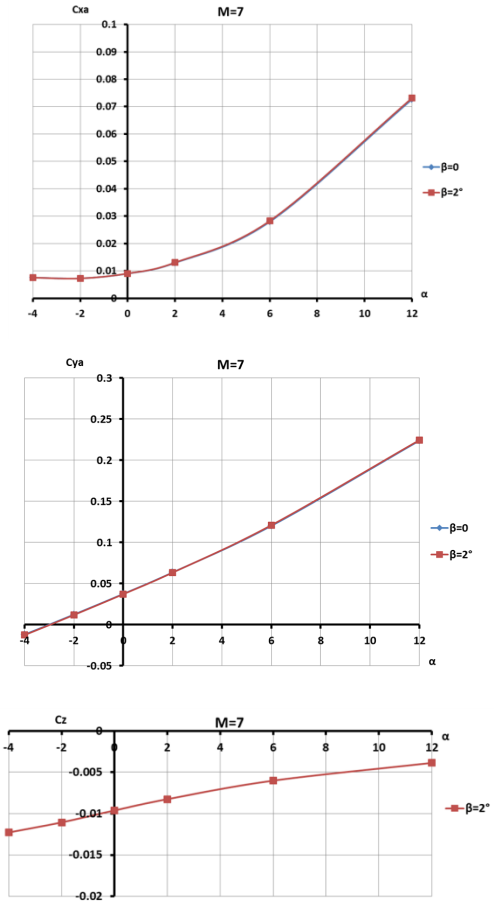

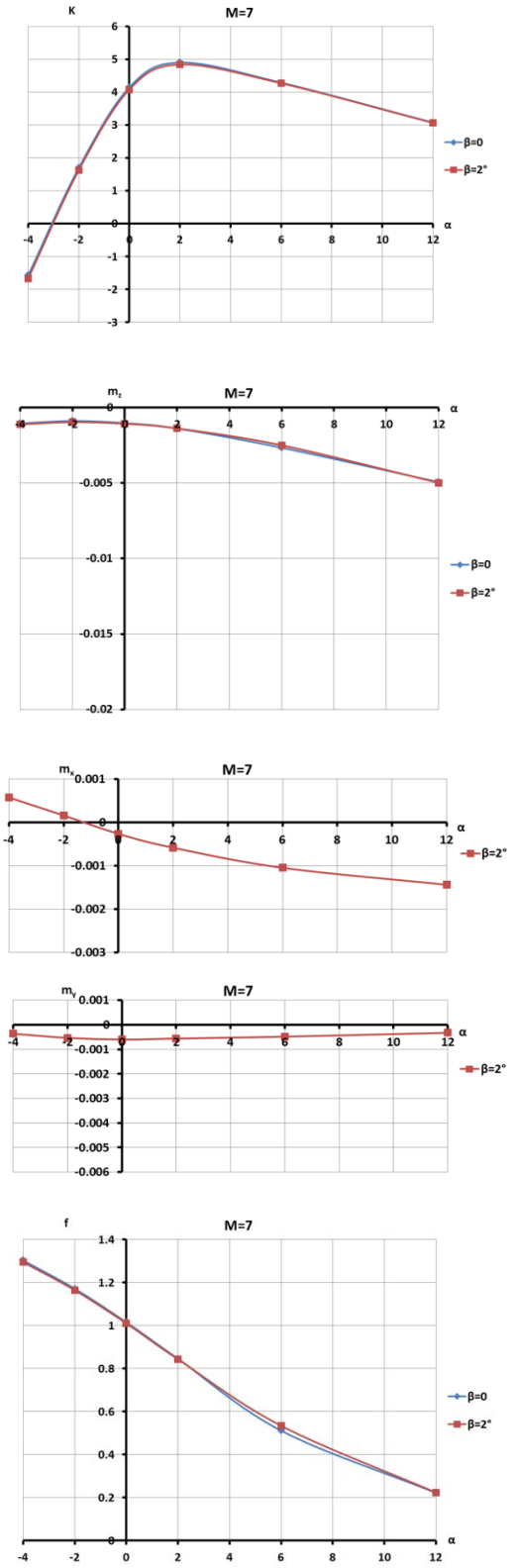

Fig. 4. Forces and moments coefficients, $K=C_L/C_D$ and flow rate coefficient f at M=7.

As can be seen from the presented graphs, the slip angle β has a weak effect on the total aerodynamic characteristics. A small influence

was noted at Mach numbers M = 2 and 4 on the magnitude of the longitudinal force. In this case, the lateral force C_z reaches its maximum values and weakly depends on the angle of attack. In the range of Mach numbers M = 6 ÷ 7.5, the nature of the $C_z(\alpha)$ and $m_y(\alpha)$ dependences varies. The lateral force C_z decreases in absolute value with increasing angle of attack, and the yaw moment coefficient m_y takes values close to zero.

Examples of flow fields obtained as a result of numerical simulation at M = 2 and 7, α = 0, β = 0, are shown in Fig. 5.

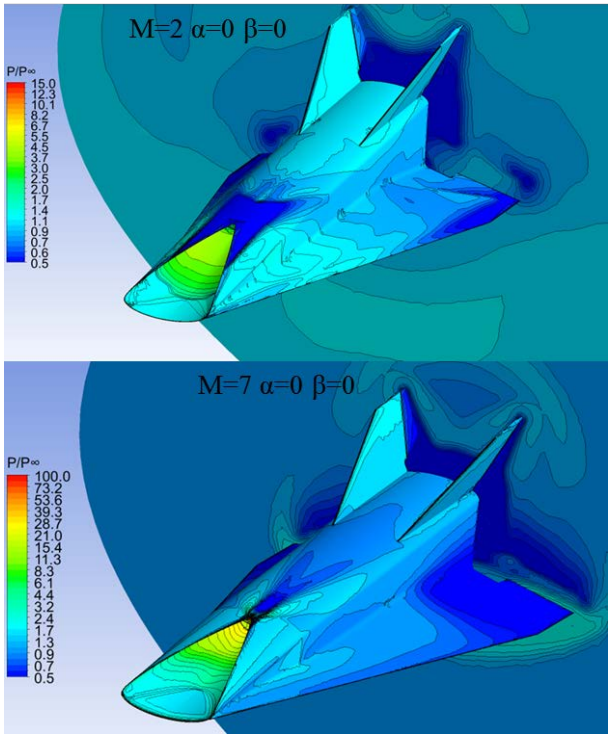

Fig. 5. Flow fields around EFTV at M=2 and 7.

The intake mass flow rate coefficient for Mach numbers M = 2, 4 takes values f = 0.1 ÷ 0.4, which indicates that the air intake device has not been started. Analysis of the flow fields showed that the main feature of this intake is the presence of subsonic zone which is formed on the center of the air intake domain practically at all flow regimes. When the Mach number M = 2 ÷ 4 subsonic flow zone is most pronounced and it formes at a distance of approximately $0.1L_{ref}$ from the leading edge and extends upstream until the intake entrance. An example of such a development of the flow is shown in Fig. 6. The change of the angle of attack practically does not affect the nature of the flow and the size of the subsonic region in the vicinity of the intake braking surface.

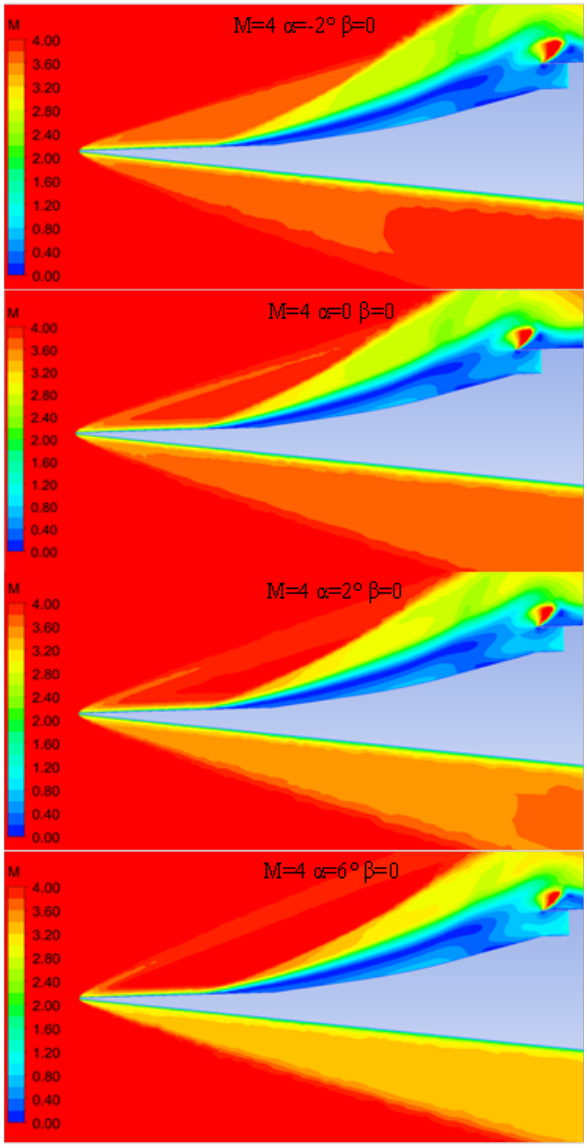

Fig. 6. Flow in intake area.

An increase in the Mach number to M = 6 substantially changes the flow pattern. At angles of attack α = -2 °, 0, the region of subsonic flow is practically absent, and begins to form at positive angles of attack (Fig. 7). A similar picture of the flow is realized at larger Mach numbers also.

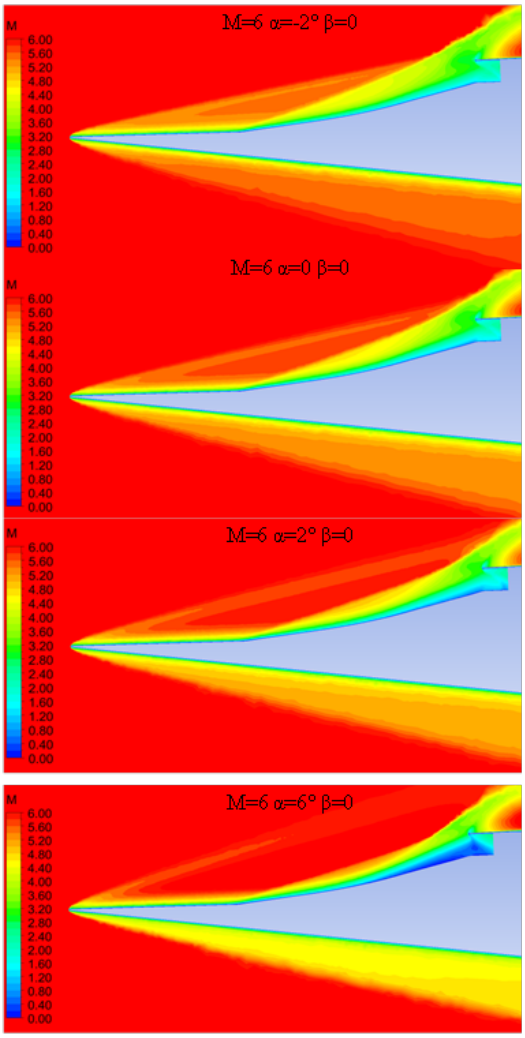

Fig. 7. Flow in intake area.

The streamlines make it possible to see in more details the structure of the flow in the vicinity of the intake compression surface. At Mach numbers M = 2 and 4, large detachment regions with backflow occur within the air intake (Fig. 8), and a significant part of the flow flows outwards. The presence of a sideslip angle β significantly changes the flow pattern inside the air intake. The most noticeable effect is observed at Mach numbers M = 2 and 4. The subsonic region is shifted to the intake leeward side, while the separation region with the reverse flow on the windward side disappears, and the flow becomes more uniform. With an increase in the Mach number, the effect of the slip angle β on the flow structure is preserved, while the subsonic zone shifting to the intake leeward side is substantially reduced.

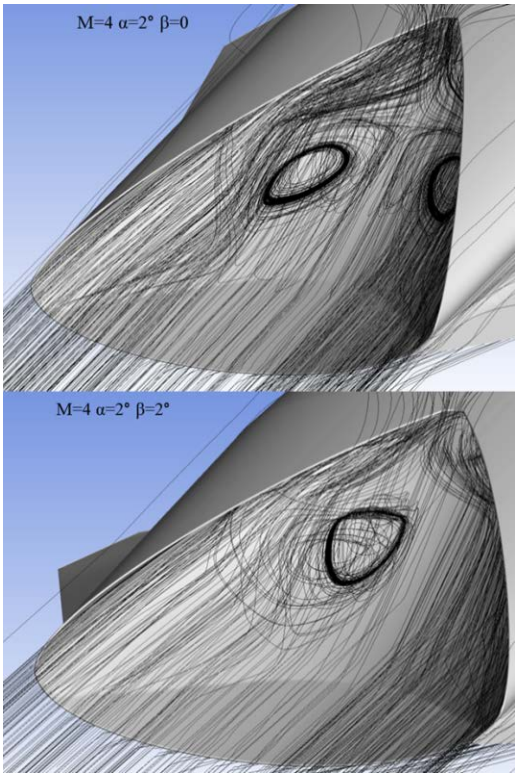

Fig. 8. Flow in intake area.

4 Experimental Research

Experimental research on aerodynamics of the EFTV powered option at Mach numbers 7 and 8 had been provided in TsAGI supersonic and hypersonic wind tunnel T-116. The scale of the aerodynamic model was 35 % to the real size of the flight test vehicle, so the length of the model was approximately 1 m. The model was made with the internal duct in order to investigate the intake characteristics and to take into account the influence of the engine duct on external aerodynamics of the vehicle including the influence of air spillage before the intake entry.

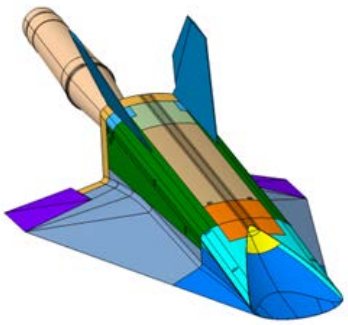

Fig. 9. Composition of the Aerodynamic Model

Composition of the model and the photo of the model installed in the test section of the wind tunnel T-116 are shown on Figs. 9 and 10.

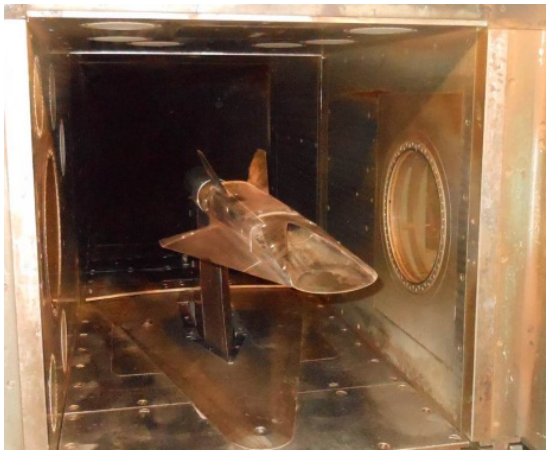

Fig. 10. The Model Installed in the Wind Tunnel T-116

The internal duct of the model simulated the intake configuration up to its throat. The other parts of the duct were modified as compared to the real engine components. At some distance from the intake throat the duct was made with the expanding cross-sectional area, and then with the constant one. The nozzle of the model duct was composed of two parts having contracting and constant cross-sectional areas ensuring a uniform exit flow with sonic velocity. Such a configuration of the internal duct allows determining the intake mass flow rate and the nozzle exit flow momentum by measurement of total and static pressures and total temperature in the exit section of the nozzle by the special rake combining a number of total and static pressure probes and thermocouples. Configuration of the internal duct of the model and the position of the measurement rake are shown in Fig. 11.

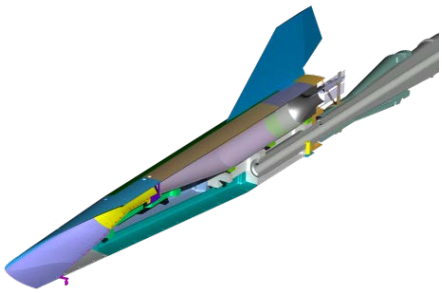

Fig. 11. Configuration of the Internal Duct of the Model and the Measurement Rake

In order to study the influence of the intake throat area on the intake starting performance, the model was manufactured with two variants of the intake throat: the original one corresponding to the EFTV configuration with the contraction ratio CR = 8.6, and the expanded throat with CR = 7.4 (CR being the ratio of the intake capturing area to the area of the intake throat). These two variants of the intake throat were ensured by two replaceable inserts shown in Figures 9 and 11 by yellow color.

The results of tests presented, in particular, in Refs [6], [7] and [8] showed that start of the intake depends from both the intake contracting ratio CR and the boundary layer (BL) state on the intake surface. In the wind tunnel T-116, the intake started just with the expanded throat area, and installation of the transition grit generating a number of vortices near the intake compression surface promoted early BL transition and significantly improved the intake starting performance. Configurations of different transition grits used are shown on Fig. 12.

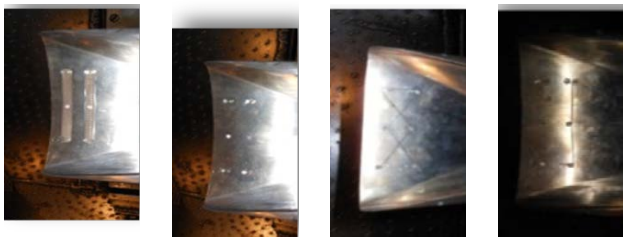

Var. 1 Var. 2 Var. 3 Var. 4

Fig. 12. Different Variants of the BL Transition Grit

These included: 2 metallic strips with 3 rows of diamond-shaped roughness elements each; the heights of the roughness elements were 0.75 mm and 1 mm (variant 1), 10 screw heads of a ‘dovetail’ shape having the height k=1.2 mm and the top diameter D = 3.8 mm installed at distances of approximately 15 mm and 35 mm from the leading edge of the intake at three positions dispersed by the lateral co-ordinate (variant 2), the same screw heads with wires of the diameter d = 0.5 mm attached to the model surface by the screws in ‘cross’ position (variant 3) and in ‘lines’ parallel to the intake leading edge (variant 4). The tests were provided at Mach numbers 7 and 8.

The results of tests showed that the intake without transition grit started just in very limited range of test flow condition: the intake didn't start at Mach number 7 at all, and starting observed just at Mach number 8 and negative angles-of-attack $\alpha \leq -1°$. The test results obtained at Mach number 8 in terms of the intake mass flow rate f dependencies from angle-of-attack α obtained at Mach number 8 for 'pure' model and for the model with transition grits, variants 1 and 2 are presented in Fig. 13. The Reynolds number during the M=8 tests was $Re_{1m} = 5.92 \cdot 10^6$ and corresponded to the real EFTV flight altitude H = 32.5 km. It is seen that the transition grit variant 1 didn't improve the situation, and the grit variant 2 consisting of 10 screw heads widened the range of the intake starting up to positive angles-of-attack $\alpha \leq 2°$.

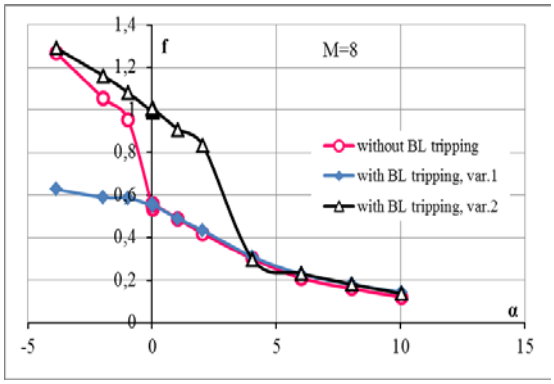

Fig. 13. The Intake Mass Flow Rate Coefficient f vs. Angle-of-Attack α, M = 8

The tests of the model at Mach number 7 were provided with different transition grits, variants 2, 3 and 4. Reynolds number during the most of tests at M = 7 was $Re_{1m} = 7.22 \cdot 10^6$; the corresponding flight altitude being H = 30 km. In addition, one test with $Re_{1m} = 4.22 \cdot 10^6$ (H = 34 km) for the model with the transition grit variant 2 was made. The test results on the intake mass flow rate coefficient are shown on Fig. 14.

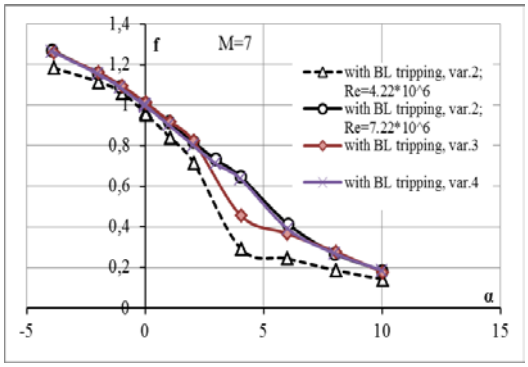

Fig. 14. The Intake Mass Flow Rate Coefficient f vs. Angle-of-Attack α, M = 7

As it is seen from the presented results, additional wires in compositions of the transition grits, variants 3 and 4 did not displayed positive impact on the intake starting. Taking the latter into account, the variant 2 of the transition grit chose as the main one for further aerodynamic tests.

For measurement the aerodynamic forces and moments acting on the model, the electro-mechanical balance of T-116 was used. In order to obtain external aerodynamic characteristics of the model, correction on internal aerodynamic drag was subtracted from the test results. The absolute value of this correction was calculated as a difference between the values of the exit flow momentum exhausting from the internal duct of the model and the initial momentum of the stream-tube entering to the intake (in the free-stream area), both values calculating from measurement of the exit flow parameters by the rake shown on Fig. 11. The correction was introduced in the body reference frame along its longitudinal axis. As a result, components of the external aerodynamic force obtained included, apart from aerodynamic forces acting on external surfaces of the model, the influence of the flow spillage taking place near the intake crotch. The pattern of the spillage could be seen from the CFD flow-field depicted on Fig. 15.

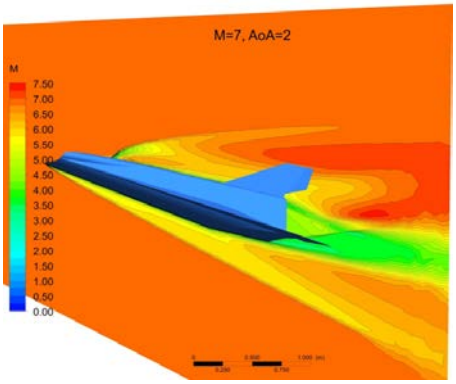

Fig. 15. The pattern of the spillage

Correction on the internal drag multiplied by the arm of the exit nozzle axis to the adopted center-of-gravity of the model was introduced also to the pitching moment acting on the model and measured by the balance. By so doing, the pitching moment obtained includes the impacts of the external surface of the model, of flow spillage before air intake, and of the momentum of the flow entering to the intake. In order to get the resulting pitching moment acting on the real aircraft or test vehicle with operating or non-operating scramjet, it will be sufficient to add just the impact of the exit flow to the pitching moment obtained from the experimental data processed by the described procedure.

The balance tests on external aerodynamic characteristics of the model were provided just with the expanded throat area of the intake (CR = 7.4), without and with the BL tripping grit, variant 2 consisting of 10 screw heads, with different flaps deflection. The main test results obtained at Mach number M=7 for drag force coefficient C_D, lift force coefficient C_L, aerodynamic efficiency L/D, and pitching moment coefficient C_m with symmetrical right and left flaps deflection (R_fl = L_fl = 0, -6° and -12°) are presented in Figs. 16 to 19. For comparison, on Figs. 18 and 19 the aerodynamic efficiency and the pitching moment coefficient C_m dependencies obtained with unstarting intake (without BL tripping) are also presented.

The results of aerodynamic tests of the model obtained at Mach number 7 and processed as described above are presented on Figs. 16 to 19. Reference values of the characteristic area and length, as well as center-of-gravity position, are the same as used in CFD research.

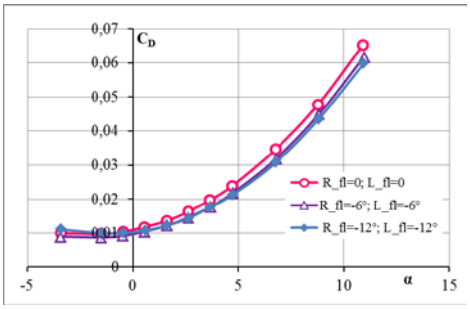

Fig. 16. Experimental Results on the External Drag Force Coefficient C_D vs. Angle-of-Attack α, M=7

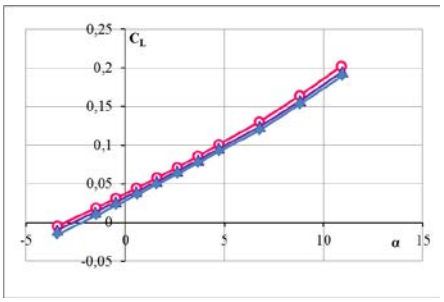

Fig. 17. Experimental Results on the Lift Force Coefficient C_L vs. Angle-of-Attack α, M=7

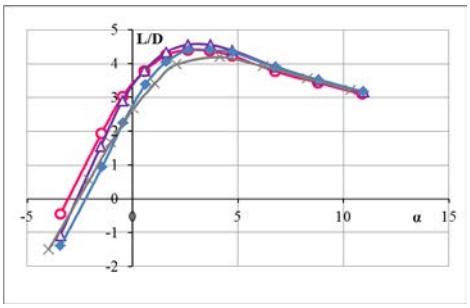

Fig. 18. Experimental Results on the Aerodynamic Efficiency L/D vs. Angle-of-Attack α, M=7

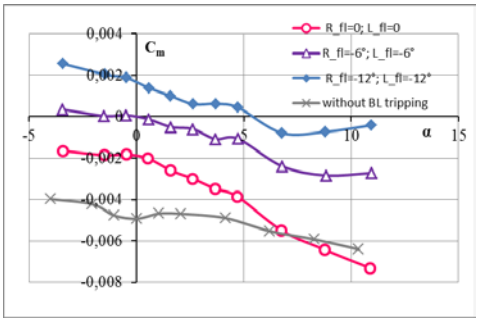

Fig. 19. Experimental Results on the Pitching Moment Coefficient C_m vs. Angle-of-Attack α, M=7

It is seen from the experimental results that the maximum value of aerodynamic efficiency L/D of the model is about 4.5, and the vehicle with transition grit could easily be trimmed by flaps deflection on -6° provided that the exit flow exhausting from the scramjet

engine nozzle will not produce significant pitching moment.

It could be seen also that unstart of the intake will lead to significant change in the pitching moment coefficient especially at low angles-of-attack. At angles-of attack $\alpha \geq 5°$ where the intake in any case does not start, the influence of the transition grit is minimal.

6 Conclusions

The numerical simulation and experimental studies of the flow around the high-speed civil aircraft model HEXAFLY-INT and in the air intake device have been performed.

Conducted CFD and EFD studies of the flow in the area of the air intake of high-speed aircraft model HEXAFLY-INT have shown that one of main feature of this configuration is the occurrence of subsonic separation zone in the central part of flow in this intake. This feature influences both on the intake performances and on external aerodynamics.

Maximum value of aerodynamic efficiency L/D of the model is about 4.5. Unstart of the intake will lead to significant change in the pitching moment coefficient especially at low angles-of-attack.

Acknowledgements

This work was performed within the 'High Speed Experimental Fly Vehicles - International' (HEXAFLY-INT) project fostering International Cooperation on Civil High-Speed Air Transport Research. HEXAFLY-INT, coordinated by ESA-ESTEC, is supported by the EU within the 7th Framework Program Theme 7 Transport, Contract no.: ACP3-GA-2014-620327. The project is also supported by the Ministry of Industry and Trade, Russian Federation. Further information on HEXAFLY-INT can be found on http://www.esa.int/techresources/hexafly_int.

References

[1] Steelant J, Varvill R, Defoort S., Hannemann K, and Marini M.: "Achievements Obtained for Sustained Hypersonic Flight within the LAPCAT-II project", 20th AIAA International Space Planes and Hypersonic Systems and Technologies Conference, Glasgow, Scotland,July 6–9, 2015:AIAA-2015-3677.

[2] Steelant J. and Langener T.: "The LAPCAT-MR2 hypersonic cruiser concept", 29th Congress of the International Council of the Aeronautical Sciences (ICAS), St. Petersburg, September 7 – 12, 2014.

[3] Steelant J, Langener T, Di Matteo F, Hannemann K, Riehmer J, Kuhn M, Dittert C, Scheuerpflug F, Jung W, Marini M, Pezzella G, Cicala M and Serre L.: "Conceptual Design of the High-Speed Propelled Experimental Flight Test Vehicle HEXAFLY", 20th AIAA International Space Planes and Hypersonic Systems and Technologies Conference, Glasgow, Scotland, July 6 – 9, 2015: AIAA-2015-3539.

[4] Meerts C, and Steelant J.: "Air Intake Design for the Acceleration Propulsion Unit of the LAPCAT-MR2 Hypersonic Aircraft", 5th European Conference for Aeronautics and Space Sciences (EUCASS), Munich, July 1 – 5, 2013.

[5] Крайко А.Н. Теоретическая газовая динамика: классика и современность. – М.: ТОРУС ПРЕСС, 2010.

[6] Voevodenko NV, Gubanov AA, Ivaniushkin DS, Lunin VYu, Gusev DYu, Ivankin MA, Talyzin VA, and Yakovleva VA: "Numerical and experimental studies of the flow on HEXAFLY-INT experimental flight test vehicle air intake", 20th AIAA International Space Planes and Hypersonic Systems and Technologies Conference, Glasgow, Scotland, July 6 – 9, 2015: AIAA 2015-3584.

[7] Voevodenko NV, Gubanov AA, Gusev DYu, Ivankin MA, Ivanyushkin DS, Lunin VYu, Meshennikov PA, Talyzin VA, Shvalev YuG, and Yakovleva VA: "Boundary layer state influence on start of the inward-turning intake", 30th Congress of the International Council of the Aeronautical Sciences (ICAS), Daegeon, Korea, September 26 – 30, 2016.

[8] Gubanov AA, Guryleva NV, Ivankin MA, Talyzin VA, Voevodenko NV, and Yakovleva, V.A.: "Experimental research of the inward-turning intake starting at TsAGI T-116 wind tunnel within the international HEXAFLY-INT project", 7th European Conference for Aeronautics and Space Sciences (EUCASS), Milan, Italy, July 3 – 6, 2017.

Contact Author Email Address

The contact author is Nina Voevodenko, TsAGI, whose e-mail is nina.voevodenko@tsagi.ru .

Copyright Statement